

# Line-broadening studies of excited diatomic homoatomic and heteroatomic Rydberg molecules formed by potassium, rubidium, and cesium atoms

C. Vadla,<sup>1</sup> V. Horvatic,<sup>1,\*</sup> and K. Niemax<sup>2</sup><sup>1</sup>*Institute of Physics, Bijenicka 46, 10000 Zagreb, Croatia*<sup>2</sup>*ISAS–Institute for Analytical Sciences, Technische Universität Dortmund, Bunsen Kirchhoff-Strasse 11, 44139 Dortmund, Germany*

(Received 30 July 2009; published 19 November 2009)

Recent absorption measurements of the self-broadening of Rb principal series lines [C. H. Greene, E. L. Hamilton, H. Crowell, C. Vadla, and K. Niemax, *Phys. Rev. Lett.* **97**, 233002 (2006)] verified the existence of minima in highly excited long-range potentials of Rb<sub>2</sub> which were predicted theoretically as bound Rydberg molecule [C. H. Greene, A. S. Dickinson, and H. R. Sadeghpour, *Phys. Rev. Lett.* **85**, 2458 (2000)]. The present paper reports on the extension of these experimental studies to principal series lines of K broadened by K as well as Cs broadened by Cs. In addition, the broadening of some lower members of the K, Rb, and Cs principal line series due to heteroatomic interactions was investigated. The analysis of the measured satellite structures in the quasistatic line wings and their comparison to the previously published analogous data for Rb\*+Rb system lead to the conclusion that one can expect existence of potential minima in homo- and heteroatomic alkali-metal  $A^*+B$  systems in a wide range of principal quantum numbers, starting with K, Rb, and Cs excited to the third resonance states. The positions and strengths of the satellite structures indicate that the potential minima are due to scattering of the valence electron by ground-state perturbers.

DOI: [10.1103/PhysRevA.80.052506](https://doi.org/10.1103/PhysRevA.80.052506)

PACS number(s): 33.15.-e, 32.80.Ee, 32.30.Jc, 32.70.Jz

## I. INTRODUCTION

Recently, bound trilobite and butterfly Rydberg molecules, a new class of exotic molecules, gained significant attention. Such molecules were postulated by Greene *et al.* [1–3] and Khuskivadze and co-workers [4] some time ago. They can be formed in collisions between two [1–4] or also more [5] very cold atoms where one atom is in a highly excited Rydberg state and the other atoms in their ground states. The binding of the very slow atoms is due to the slow Rydberg electron, which, in the case of dimers, is scattered from a ground-state atom with negative scattering length. The spatial distributions of the electron density in such states look like trilobites or butterflies with strong maxima at the position of the scattering ground-state atom [2]. The resulting Born-Oppenheimer potential curves oscillate like electron wave functions. In the case of such highly excited Rydberg atoms, several approximations can be made, including the interaction potential, which can be taken in the form of a Fermi pseudopotential [1–3]. Highly excited Rydberg molecules are especially interesting because of their unique properties, e.g., large size and long lifetimes, which scale with powers of the principal quantum numbers  $n$  or, more precisely, with powers of the effective principal quantum number  $n_{eff}$ . However, the predicted Rydberg molecular bonds are weak since the potential depths amount only to a small fraction of the spacing between neighboring  $n$  manifolds. For example, binding energies of about 12 GHz ( $0.4\text{ cm}^{-1}$ ) were calculated for “trilobite” Rb<sub>2</sub>\* formed by Rb\* in low  $l$  states at  $n=30$  and Rb in the ground state [1–3]. The internuclear separation at the binding minima of these potentials was predicted to be of the order of 1250 a.u., i.e., 66 nm.

A direct experimental verification of this new class of giant, bound Rydberg molecules would require an atomic ensemble cooled near to absolute zero temperature, e.g., in an atomic trap, and direct or stepwise laser excitation of the vibrational levels in the potential wells of the excited molecules. However, the first experiment, which pointed out that such molecules can be formed, was made in our laboratory [6] at thermal conditions and for intermediate Rydberg states. It was a relative simple absorption experiment in hot and dense Rb vapor where the satellites in the quasistatic wings of self-broadened Rb principal series lines (transitions  $5^2S_{1/2}-n^2P_J$ , henceforth labeled as  $nP$ ) were studied. Line broadening experiments determining the positions of satellites are known to be an excellent tool for the measurement of extrema in molecular difference potentials [7,8]. Within the limits of experimental uncertainty, very good agreement was found between the positions of the Rb line satellites and the predicted potential depths of the Rb<sub>2</sub>\* Rydberg molecules.

The first verification of the new class of molecules by the line-broadening experiment in Rb is also indicating that similar satellites found in absorption spectra of self-broadened Cs principal series lines a long time ago [9–11] have the same origin. Analogous regularities in the spectra of rubidium vapor were observed at that time as well, but were not published (see remark given in [11]). The formation of these satellites remained unexplained in the same way as the strong oscillations of the collision cross sections of alkali-metal Rydberg atoms by alkali-metal ground-state atoms in dependence on principal quantum number [11,12]. Neither *ab initio* nor the usual long-range perturbation calculations provide any explanation for the clearly pronounced satellite structures in the quasistatic wings of the third and higher alkali-metal resonance lines. Different models proposed did not lead to satisfactory explanation of this issue. Note that full *ab initio* calculations of the relevant molecular Rydberg states are very difficult using existing quantum chemistry

\*Author to whom correspondence should be addressed; blecic@ifs.hr

programs because of the large number of coupled states and large electron distances involved. This is the reason why no *ab initio* potentials have been published yet, which are relevant for the lines investigated in the present work. There was the attempt to correlate these experimental findings with the scattering phase shifts of the Rydberg electron on the ground-state perturber atoms by Fabrikant [13] with some success. However, this problem needs to be revisited in the light of the new understanding of Rydberg molecules.

Very recently, the stepwise laser excitation of vibrational levels in ultracold  $\text{Rb}_2^*$  Rydberg states has been performed in a beautiful trap experiment with field-ionization detection of the excited molecules [14]. The agreement with theoretical predictions of  $\text{Rb}_2^*$  Rydberg potential for values of  $n$  ranging between 33 and 40 was very good. This experiment can be regarded as a final evidence for the existence of the butterfly Rydberg molecules.

The present paper reports on the extension of the earlier Rb line-broadening measurements [6] to pure K and Cs vapors. Self-broadening measurements of the K  $nP$  series ( $n=5-12$ ) have not been reported before, while the investigation of the Cs principal series lines is a repetition of the earlier experiment in 1983 [11]. Furthermore, in order to study the potential depths of heteroatomic Rydberg molecules, satellite features in the wings of the K  $6P$  and Cs  $8P$  lines broadened by Rb as well as of the Cs  $8P$ ,  $9P$  and the Rb  $7P$ ,  $8P$  lines broadened by K were measured.

## II. EXPERIMENT AND METHOD

To get measurable absorption signals in the quasistatic wings of the higher alkali-metal principal series lines, one has to generate metal vapor columns with atom number densities up to  $10^{18} \text{ cm}^{-3}$  (pressure: up to 200 mbar) at column lengths of about 10 cm. There are no cells with optical windows, which are resistant to the corrosive influence of such hot and dense alkali-metal vapors. The technical problem can be easily circumvented by the use of heat pipes where the buffer gas serves for window protection. However, in the transition zones between the hot metal vapor column and cold buffer gas layers, the vapor is inhomogeneous and, in addition, alkali-metal clusters are formed. At pressures up to  $\sim 20$  mbar, the clusters are acting as a stable gray filter, but at higher pressures a turbulent cluster fog strongly perturbs the transmitted light intensity. In the case of potassium, simultaneously with the turbulent cluster fog, solid weblike structures are formed in the transition regions, which are rapidly growing at higher pressures, completely obstructing the light transmission within a few hours. The mentioned difficulties can be efficiently removed by a long, thin inner heater placed in the heat pipe axis. This and other details of our experimental arrangement (Fig. 1) are given in an earlier paper [15]. However, for reader's convenience, it will be briefly described here again.

The heat pipe was made of an 18-cm-long stainless-steel tube having 2 cm inner diameter. The central part of the tube with the metal bath was heated resistively by an outer heater (maximum power: 500 W). The side arms were cooled by water and the recirculation of the liquid metal was accom-

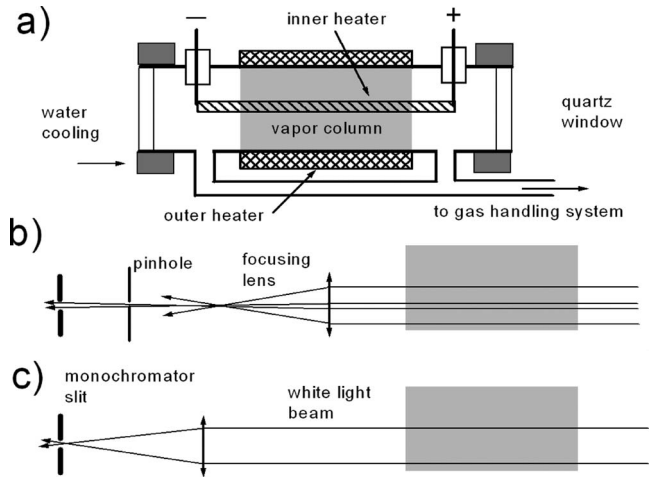


FIG. 1. Sketch of the experimental arrangement (not in scale). (a) Heat pipe with built-in heater for suppression of cluster formation and weblike solidification of alkali metal in the transition zones between the vapor column and buffer gas layer. (b) Optical arrangement for spatially resolved measurements and (c) for spatially non-resolved measurements.

plished by a stainless-steel mesh. The vapor column length was  $L=(6 \pm 0.5) \text{ cm}$  so that the quartz windows at both ends were separated by  $\sim 3 \text{ cm}$  long buffer gas (Ar) layers from the hot vapor. The inner heater was made of Mo wire (thickness:  $250 \mu$ ) wound up to a helix (length: 15 cm, diameter: 2 mm, resistance:  $2 \Omega$ ). Molybdenum was chosen because of its chemical resistance to hot and dense alkali-metal vapors.

For example, cluster fogs and weblike solid structures in the intermediate zone can be completely suppressed applying moderate inner heating powers (about 10 W) at  $\sim 100$  mbar which is a typical alkali-metal vapor pressure in the present experiment. However, the radial temperature distribution  $T(r)$  of the generated stable vapor column is inhomogeneous in the heat pipe, i.e., it monotonically varies from the higher temperature  $T_{\text{ih}}$  at the inner heater to the lower metal bath temperature  $T_w$  at the heat pipe wall. These boundary temperatures depend on the heating powers applied and, in turn, on the established vapor density. The vapor density was mainly influenced by the outer heating. An increase of the vapor density improves the thermal conductivity of the heat pipe and, consequently, cools the inner heater.

The metal vapor number density  $N(w)$  near the heat pipe wall is governed by  $T_w$  via the corresponding vapor pressure curve. At distance  $r$  from the heat pipe axis, the vapors are overheated and, according to Dalton's law, the number density  $N(r)=T_w N(w)/T(r)$ . This yields an opportunity to measure the temperature dependence of the molecular and quasi-molecular spectral features by spatially resolved absorption measurements at various  $r$  positions of the heat pipe diameter.

Spatially resolved measurements were performed in a similar manner as reported in [15], where the red and infrared potassium spectra were investigated. The spectra are taken from thin absorption columns of diameter  $dr \approx 0.5 \text{ mm}$  at given distance  $r$  from the heat pipe axis which

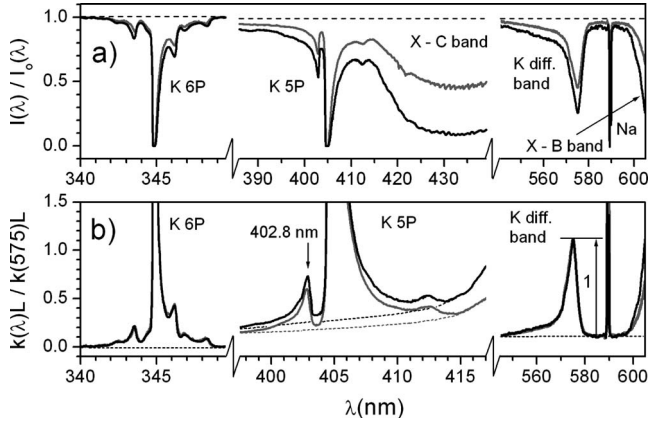


FIG. 2. (a) Parts of the spatially resolved absorption spectra of an overheated potassium vapor measured near to the inner heater (gray lines) and near to the heat pipe wall (black lines). The number densities and temperatures near to the inner heater were  $4.8 \times 10^{17} \text{ cm}^{-3}$  and 1000 K, respectively, while the corresponding values near to the heat pipe wall were  $5.9 \times 10^{17} \text{ cm}^{-3}$  and 815 K. The argon buffer gas pressure (70 mbar) was somewhat higher than the potassium vapor pressure (66 mbar), so that the heat pipe was running near the heat pipe mode. (b) Relative reduced absorption coefficients measured with respect to the peak absorption of the K diffuse band at 575 nm. The presented data show the temperature independence of the blue satellite of the second K resonance doublet at 402.8 nm and satellite structures in the vicinity of the third principal series line.

is determined by the imaging of the collimated white light beam incident onto the entrance slit of the monochromator as shown in Fig. 1(b). The spectra were measured using a 0.5 m Jarrell-Ash monochromator (band pass: 0.03 nm at 400 nm) supplied with an RCA 1P28 photomultiplier. The light source was a 25-W halogen lamp (Osram) with nondoped quartz window yielding a measurable continuous spectrum down to about 280 nm. The spatially resolved measurements reduce significantly the incident light intensity, i.e., the detection sensitivity. In particular, this was the problem for the measurements below 320 nm where the uv radiation intensity of the used halogen lamp strongly decreased. To increase the signal-to-noise ratio, the measurements below that limit were performed without spatial resolution [see sketch in Fig. 1(c)] and the average absorption spectra in the space between the heat pipe axis and the heat pipe wall were registered. Typical spatially resolved spectra in dense potassium vapors, comprising the second and third K resonance transitions together with the K diffuse band are shown in Fig. 2.

The partial absorption spectra displayed in Fig. 2(a) were measured at two extreme positions: near the inner heater and near the heat pipe wall. As shown in [15], the potassium diffuse band with the peak intensity at 575 nm can be used as reliable standard for determination of the potassium atomic number density in dense potassium vapors.

Within the semiclassical approach, the wavelength- and temperature-dependent reduced absorption coefficient  $k_R = k(\lambda, T)/N^2$  of a molecular band can be described by well-known quasistatic formula [7,8]

$$k_R(\lambda, T) = \frac{4\pi^2 e^2 h}{m_e c} \sum_{m,n} \sum_C f_{nm}(R_C) \frac{R_C^2}{|dE_{mn}/dR_C|} \exp[-\Delta E_n/k_B T]. \quad (1)$$

Here, the Boltzmann constant is labeled by  $k_B$ , while  $m_e$ ,  $c$ ,  $e$ , and  $h$  have their usual meanings. The first summation is related to all relevant difference potentials  $E_{mn}(R) = E_m(R) - E_n(R)$  between the upper  $m$  and lower  $n$  molecular states at given interatomic distance  $R$  of the interacting atom pair. Formula (1) is valid for the regions where no extrema in difference potentials occur. The second summation is over all Condon points  $R_C$  for which the classical Franck-Condon condition  $E_{mn} = hc/\lambda$  is satisfied. The  $R$ -dependent atomic oscillator strength for a particular  $n \rightarrow m$  transition is labeled by  $f_{nm}(R)$ . The temperature dependence of the absorption coefficient is determined by the exponential Boltzmann factor comprising the differences  $\Delta E_n(R) = E_n(R) - E_n(\infty)$  between the lower potentials at distance  $R$  and their asymptotic values  $E_n(\infty)$ . In the case of the potassium diffuse band at 575 nm, the lower molecular state is represented by the shallow triplet interaction potential  ${}^3\Sigma_u^+$  for which at thermal conditions  $\Delta E_n \ll k_B T$  [15]. Thus, the absorption coefficient of the potassium diffuse band is practically independent on temperature at thermal conditions, i.e.,  $k(575) \propto N_K^2$ . Dividing the measured optical depths  $k(\lambda, T)L$  by the optical depth at the peak of the diffuse band  $k(575)L$ , one obtains the relative reduced absorption coefficients  $k(\lambda, T)L/k(575)L \propto k(\lambda, T)/N_K^2$ , which reflect the temperature dependences of particular absorption features [see Fig. 2(b)]. The measured reduced absorption coefficients can be obtained in the absolute values by using the absolute value  $k_R(575) = 3.6 \times 10^{-37} \text{ cm}^5$  reported in [15]. This simple but accurate method for quantitative evaluation of the recorded spectra has an additional, important advantage. Namely, the error due to uncertainty of the optical path  $L$  along the heat pipe cancels out in this evaluation procedure.

### III. $K^*(nP) + K$ SYSTEM

There is a long history of far-wing broadening experiments in alkali-metal vapors, which were performed to check the quality of theoretical interaction potentials. This concerns particularly the lowest principal series line including the resonance lines [7,8]. These experiments were made at moderate number densities which can be determined, e.g., from the integrated absorption of lines with known oscillator strengths. However, the present measurements required high number densities where such measurements are difficult because of molecular background absorption. Here, the wings of the first resonance lines could be used as reliable spectroscopic standards for the alkali-metal atom number density determination [15,16] in relatively dense vapors. Regarding the theory of the molecular potentials, there is a smooth transition between *ab initio* calculations and perturbation approach. *Ab initio* calculations can give a satisfactory explanation of the satellite structure of the second principal series line in cesium and rubidium self-broadenings [17,18].

Although the main subject of the present work was to investigate transitions between the ground and higher Ryd-

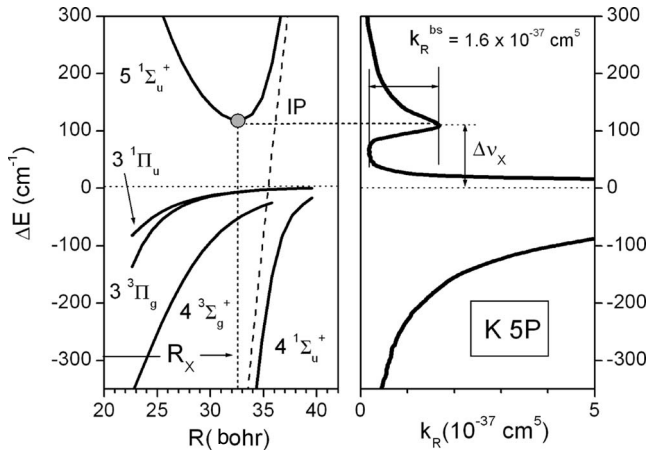


FIG. 3. (Left) Theoretical potential curves (from [19]) relevant for the transitions in the vicinity of the K 5P doublet. (Right) Reduced absorption coefficients obtained in the present experiment in respect to the center of gravity of the doublet. See text for further explanations.

berg states, here we also present the quantitative results for the reduced absorption coefficient of the second principal series line of K, which were obtained in the course of the measurements. To our knowledge, these experimental data have not been published yet. Moreover, they can serve as a test of applicability and the range where *ab initio* interaction potentials are suitable for the explanation of the satellite structures in alkali-metal principal series lines.

#### A. Second resonance doublet of potassium

Figure 3 shows the relevant K<sup>\*</sup>-K potentials for the short and medium interatomic distance  $R$  as published by [19]. The potential energy curves were calculated by an *ab initio* approach over a wide range of interatomic separation. 98 electronic states  $^{1,3}\Lambda_{g,u}^{+,-}$  adiabatically correlated with the dissociation limit  $K(4S)+K(5D)$  were taken into account. The potentials stemming from the  $K(4P)+K(6P)$  asymptotes (relevant for the transitions from the ground state) are taken from that data set and depicted in Fig. 3 (left).

At internuclear distances of interest, the ground-state  $1\Sigma_g^+$  and  $3\Sigma_u^+$  potentials (not shown here) are practically flat. In addition, the ionic potential curve IP (ground state of the  $K^++K^-$  ion pair) and the  $5^1\Sigma_u^+$  potential (asymptote:  $4S+4D$ ) are also plotted in Fig. 3. The experimental reduced absorption coefficients near the K 5P doublet are given in the right plot of Fig. 3. The data were obtained by subtracting the background of the strongly temperature-dependent potassium X-C molecular band [see Fig. 2(b)] and calibrating by the peak value of the diffuse band at 575 nm. The origin of the blue satellite of the K 5P line can be explained in the same way as it has been made for analogous satellites of the Cs 7P and Rb 6P lines in Refs. [17,18], respectively, i.e., due to avoided crossing of the ionic potential and the potentials with the same symmetry. As one can see from Fig. 3, the peak position of the blue satellite coincides with the minimum of the  $5^1\Sigma_u^+$  at  $R_x \approx 33$  a.u. Because the relevant Boltzmann factor for this satellite is  $\approx 1$  at thermal conditions,

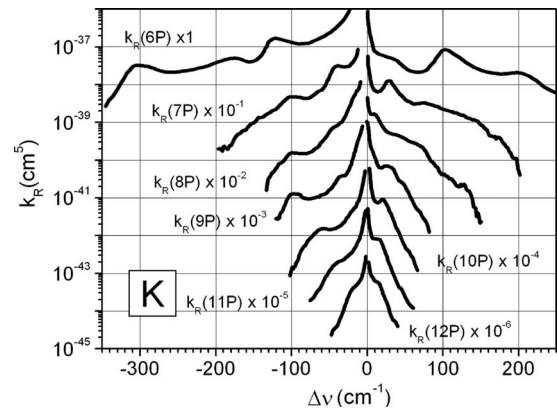


FIG. 4. The reduced absorption coefficients  $k_R(nP) = k(nP)/N_K^2$  of the self-broadened  $4S \rightarrow nP$  potassium lines. For visual clarity, the displayed reduced absorption coefficients are divided by factors of  $10^m$ . The zero-frequency detuning was set to the center of the  $4S \rightarrow nP_{3/2}$  fine-structure component.

this singlet satellite can as well be used for the determination of the potassium number density. Therefore, the most accurate value (about 10%), which is not affected by the estimation of the temperature dependent molecular X-C background, is the peak value of the satellite at the detuning  $\Delta\nu_x$  measured with respect to the absorption minimum as indicated in Fig. 3 (right).

#### B. Transitions to the higher $nP$ states ( $n > 5$ ) of potassium

The experimental reduced absorption coefficients for the wings of the potassium  $4S \rightarrow nP$  ( $n=6-12$ ) lines are given in Fig. 4. The higher members ( $n > 12$ ) of the principal series are not presented here because the absorption signals were blended due to insufficient spectral resolution of the monochromator used.

The profiles of the third ( $n=6$ ) and the fourth ( $n=7$ ) principal series doublets at 344.8 and 321.8 nm were investigated by applying the spatially resolved measurements. As demonstrated for the  $4S \rightarrow 6P$  transition in Sec. II, there is no detectable temperature dependence of the measured absorption coefficients. This means that the pronounced satellite structures in Fig. 4 occur at large interatomic separations where the ground-state potentials approach their asymptotic value and, consequently, the satellite forms reflect the shapes of the upper interaction potential curves. For the reason mentioned in Sec. II, the higher members of the potassium principal series lines were measured with no temperature discrimination.

In contrast to the first and second resonant transitions, there is no correlation between the available *ab initio* or long-range perturbation calculations and the experimental facts concerning satellite line structures for the K 6P and higher transitions. The same conclusion is valid for rubidium and cesium too. However, it was shown [6] that the satellite features for Rb  $nP$  ( $n=9-12$ ) correspond to the oscillatory long-range potential curves having the qualitative behavior that was predicted in Refs. [1-4].

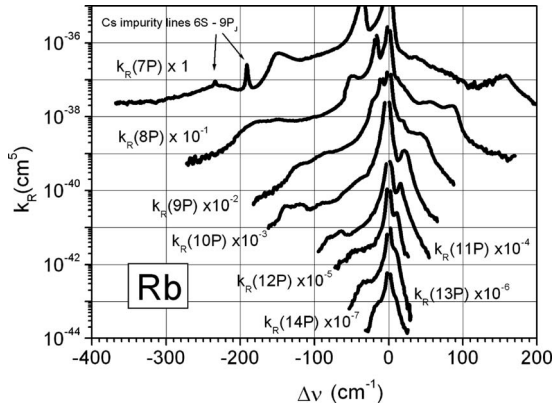


FIG. 5. The reduced absorption coefficients  $k_R(nP) = k(nP)/N_{Rb}^2$  of the self-broadened rubidium  $5S \rightarrow nP$  lines, presented in the same way as the analogous data for the potassium. Data were already published before (see Fig. 1 in [6]) and presented here for comparison to the potassium and cesium line shapes.

IV. COMPARISON OF HOMOATOMIC  $A^*(nP) + A$  ALKALI-METAL SYSTEMS

For the reader’s convenience and better representation of similarities between the line shapes of K, Rb, and Cs principal series lines, we again present in Fig. 5 our data for the reduced absorption coefficients of rubidium lines, which were already published in [6]. In Fig. 6, the analogous data for cesium taken from [11] are plotted. The only difference between the data in Fig. 6 and the first data published in [11] is the additional data for the Cs 8P line, which were obtained in the course of the present experiment.

The cesium lines were remeasured for two reasons. The first one is the check of the atomic number densities determination by the temperature insensitive molecular triplet transitions. In particular, the cesium number density was determined by the absorption coefficient of cesium diffuse triplet bands lying between 705 and 720 nm [20]. In contrast to

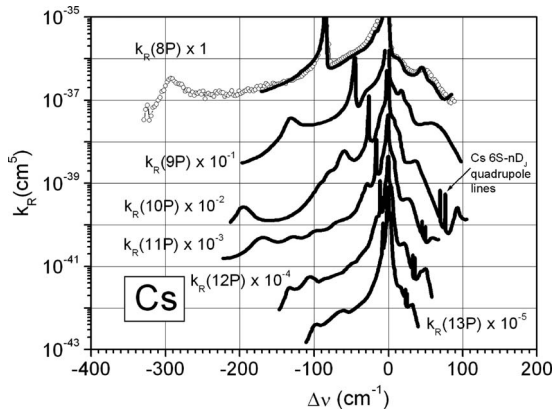


FIG. 6. The reduced absorption coefficients  $k_R(nP) = k(nP)/N_{Cs}^2$  of the cesium  $6S \rightarrow nP$  transitions. The full lines represent the profiles published in [11]. The remeasured data for the Cs  $6S \rightarrow 8P$  line obtained in the present work are labeled with open circles. The spatially resolved measurements, i.e., the measurements at various temperatures, confirmed that the feature in the far-wing of this line (not shown in [11]) belongs to the line.

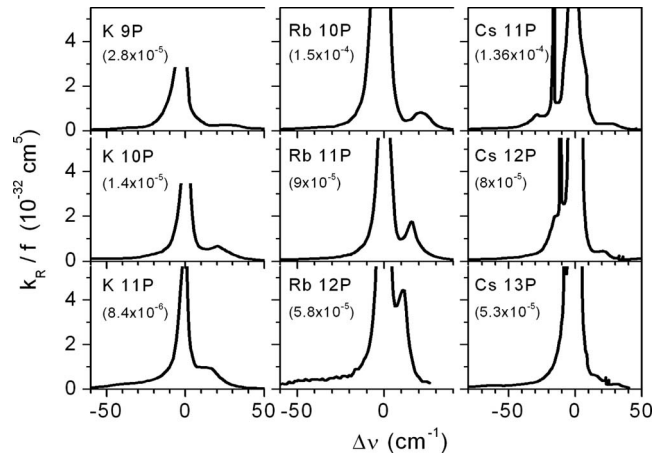


FIG. 7. Comparison of self-broadened principal series lines of K, Rb, and Cs. The effective principal quantum numbers of the vertically plotted line shapes are almost the same ( $n_{eff} \approx 7.4, 8.4,$  and  $9.4$ ). For better comparison, the values for  $k_R$  are divided by the total doublet oscillator strengths [21]. The oscillator strengths are given in brackets.

the procedure performed here, the cesium number density in [11] was determined by measuring the metal bath temperature and applying the vapor pressure curve method. The second reason was to examine the temperature dependence of the investigated satellites, which is helpful for distinguishing these spectral features from several narrow absorption bands originating from absorption transitions in the  $Cs_2$  dimer at short interatomic separation. The experimental reduced absorption coefficients obtained by both methods are in very good agreement, which is illustrated (Fig. 6) for the third self-broadened principal series line of Cs.

In general, the spectra of the self-broadened principal series lines of K and Rb are similar, especially in the case of higher series members. The satellites of the potassium lines become less structured and characterized by weak red shoulders and stronger blue satellites. In Fig. 7, the K 9P, 10P, and 11P absorption lines are compared to the analogous Rb and Cs sequences, i.e., transitions to states with nearly the same effective quantum numbers  $n_{eff}$ . The reduced absorption coefficients are given in linear scale versus frequency detuning from the centers of stronger doublet components. To make a better comparison of the satellite strengths, the reduced absorption coefficients are divided by the oscillator strengths  $f$  of the respective doublets.

Rubidium lines show the same simple form as potassium lines. The single blue satellites are even more pronounced. In contrast to that, the wings of the corresponding Cs lines do not have such simple shapes. However, as it will be shown below, cesium lines exhibit a similar simple structure for transitions to Rydberg states with higher quantum numbers.

It is instructive if the line profiles are plotted against the effective quantum  $n_{eff}$  as shown in Fig. 8. In addition to the data presented in Fig. 7, the profiles of the self-broadened Cs 20P and Cs 21P lines, taken from [11], are also plotted in Fig. 8. The wavelength scales in Fig. 8 are transformed to effective quantum number scales using the relation  $R_A/n_{eff}^2(\Delta E) = E_i - E_n - \Delta E$  for detuning dependent effective

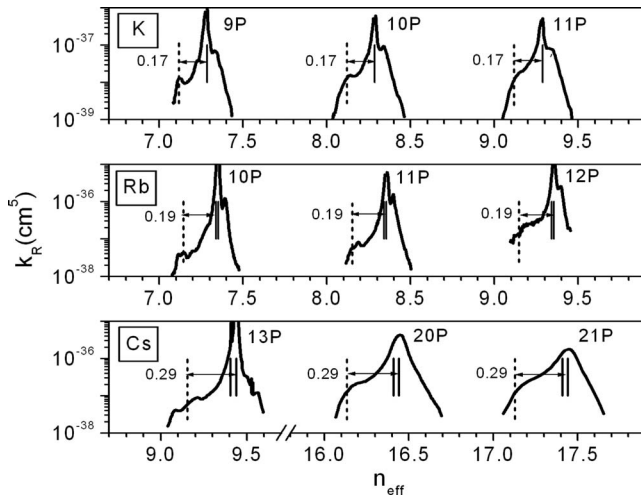


FIG. 8. Reduced absorption coefficients  $k_R$  vs effective quantum number  $n_{eff}$  for the line sequences plotted in wavelength scale in Fig. 7. The 20P and 21P Cs data are taken from [11].

quantum number  $n_{eff}(\Delta E)$ . Here,  $R_A$ ,  $E_i$ , and  $E_n$  are relevant Rydberg constants, ionization limits, and asymptotic energies, respectively. In these scales, the asymptotic energies  $E_n$  and  $E_{n+1}$  are approximately equidistant, which offers a better insight in possible regularities in the presented set of line profiles.

As one can see from Fig. 8, the cesium lines belonging to higher quantum numbers have a simple form characterized by weak shoulders in the red wings similar to the shape of potassium and rubidium lines at lower  $n$ . The  $\Delta n_{eff}$  positions of the red line shoulders with respect to the line centers are approximately the same and amount to about 0.17, 0.19, and 0.29 for K, Rb, and Cs, respectively. In the case of Rb, it was shown in Ref. [6] that strong blue satellites and weak red shoulders correspond to the minima in calculated Born-Oppenheimer potential curves arising from the scattering of the Rydberg electrons on ground-state atoms. Here, the strong blue satellites correspond to the minima of the potential curves which correlate adiabatically with close lying  $(n-1)D$  levels, while the satellite structures in the red wings are due to minima in the potential curves which dissociate into the  $nP$  asymptotes. To our knowledge, there are no  $K_2^*$  and  $Cs_2^*$  potentials available in literature which are analogous to the adiabatic potentials of  $Rb_2^*$  given in [6]. However, the regularities in the K and Cs spectra and their similarities with the Rb spectrum are implying that the corresponding potassium and cesium potentials should be similar to the available rubidium potentials. Consequently, the positions of the red shoulders of the K lines and the positions of outer Cs red satellites can be related to global minima in the corresponding potential curves. If the respective constant positions  $\Delta n_{eff}$  of the red wing shoulders in the  $n_{eff}$  plots are taken into account, the global potential minima in terms of energy are given by

$$\Delta E(n_{eff}) = \Delta n_{eff} R_y (2n_{eff} + 1) / (n_{eff}^2 + n_{eff})^2,$$

$$\Delta n_{eff} \approx \begin{cases} 0.17 & (\text{K}) \\ 0.19 & (\text{Rb}) \\ 0.29 & (\text{Cs}). \end{cases} \quad (2)$$

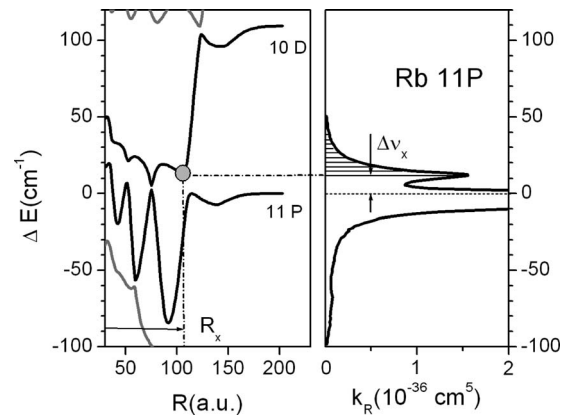


FIG. 9. Calculated Born-Oppenheimer difference potential curves of the  $Rb^*(11P)+Rb$  system compared to the reduced absorption coefficient of the quasistatic wings of the Rb 5S-11P line. The present picture is a slightly modified plot of Fig. 2 in [6].

For instance, this relation yields the values for  $\Delta E$  which are of the order of  $1 \text{ cm}^{-1}$  if formula (2) is applied for higher Rb  $nP$  states ( $n_{eff} \approx 30$ ). Such dissociation energies are predicted for  $Rb_2$  “trilobite” molecular states around  $n_{eff} \approx 30$  [1–3].

To calculate the theoretical line shape of  $k_R$ , the  $R$ -dependent oscillator strengths are needed. They have not been calculated within the framework of the investigations reported in [6]. On the other side, with the general shape of theoretical curves given [6] and known absolute values for the reduced absorption coefficient, one can estimate an average  $f(R)$  in the region of interatomic distances of interest. For this purpose, in Fig. 9 we present a modified version of Fig. 2 from [6], where the theoretical difference potential curves around the Rb 11P level and the experimental line shape are shown.

The upper difference potential (stemming from the 10D level) has a minimum at  $R_x$ , which corresponds to the blue satellite at detuning  $\Delta \nu_x$ . One can approximately assume that the contributions to the reduced absorption coefficient in the frequency region  $\nu \in (\infty, \Delta \nu_x)$  are directly related to the difference potential in the region of interatomic distances  $R \in (0, R_x)$ . In this case, Eq. (1) can be transformed to the following approximate expression:

$$\int_{\infty}^{\Delta \nu_x} k_R(\nu) d\nu \leq \frac{4\pi^2 e^2}{mc} \int_0^{R_x} f(R) R^2 dR = \frac{4\pi^2 e^2}{3mc} \overline{f(R)} R_x^3. \quad (3)$$

Here, it was taken into account that the corresponding Boltzmann factor is 1. With the theoretical value  $R_x = 108 \text{ a.u.}$  (see left plot of Fig. 9), the integration of the  $k_R(\nu)$  in Eq. (3) yields the average value for the oscillator strength  $\overline{f(R)} = 1.8 \times 10^{-5}$  for the Rb 11P line. This value amounts to 20% of the total oscillator strength of the Rb 5S-11P line ( $f_{tot} = 8.9 \times 10^{-5}$ ). The same procedure performed for the Rb 5S- $nP$  sequence  $n=9-12$  yielded the same result ( $\overline{f(R)} = 0.2 f_{tot}$ ) with an accuracy of 10%. On the other hand, one can estimate via Eq. (2) the lowest values for  $R$  at which the relevant potential minima occur without

knowing the calculated values for  $R_x$  and choosing the  $\overline{f(R)}$  values to be equal to  $f_{\text{tot}}$ . For example, in the case of Rb 11P line, this check leads to a value  $R_x^{\text{min}} \geq 63$  a.u.. It means that the experimental data themselves indicate that the investigated satellite structures are generated in the long-range interaction region. A further check for the validity of this estimation can be obtained by using the data for potassium presented in Figs. 3 and 7. By applying Eq. (2) to the blue satellites of the K 4S-10P (see Fig. 7) and K 4S-5P (see Fig. 3) lines and assuming  $\overline{f(R)}$  to be the equal to the corresponding total oscillator strength, one obtains the minimum  $R_x$  values of 60 and 15 a.u., respectively. This clearly indicates that, in contrast to the K 4S-10P line, the blue satellite of the second principal series doublet of K is due to transitions in the short-range interaction region. It has to be emphasized that the positions and strengths of the blue satellites of the considered K 9P, 10P, and 11P lines yield  $R$  values which correspond to the size of the Rydberg atom ( $R \approx 1.5 \times n_{\text{eff}}^2$ ) if Eq. (3) with  $\overline{f(R)} = 0.2f_{\text{tot}}$  is applied.

The obvious resemblance between the satellite structures of the potassium, rubidium, and cesium lines implies that in all three cases, similar interaction potentials are involved. Therefore, following the conclusions made for Rb<sub>2</sub>\* [6], electron scattering on the ground-state perturber atom is also the major mechanism for establishing the potentials of K<sub>2</sub>\* and Cs<sub>2</sub>\* with their extrema. Nevertheless, the cesium potentials are expected to be somewhat different and more complicated because the energy differences between the neighboring  $P$  and  $D$  states are smaller and the spin-orbit interaction is larger than for potassium or rubidium.

## V. HETEROATOMIC $A^*(nP)+B$ ALKALI-METAL SYSTEMS

Absorption measurements of the quasistatic wing line broadenings of potassium, rubidium, and cesium principal series lines by unlike alkali-metal ground-state atoms can serve as an additional check of theoretical modeling and may contribute to a better understanding of the processes involving Rydberg molecules. However, from the experimental point of view, there are some difficulties in the experiment, which are difficult to overcome in dense alkali-metal vapor mixtures.

To start with, the principal line series of atoms  $A$  and  $B$  in the mixture are blended and absorption measurements of only a limited number of isolated lines are possible. Furthermore, the relevant absorption signals which are due to heteroatomic reactions are mixed with homoatomic contributions. Taking into account the present experimental conditions, it is justified to assume that binary approximation is valid. Therefore, the measured absorption coefficients in the vicinity of the lines of the element  $A$  are generally of the form  $k = k_R^{AA} N_A^2 + k_R^{AB} N_A N_B$ . Here, the  $k_R^{AA}$  and  $k_R^{AB}$  label the reduced absorption coefficients due to  $A^*(nP)+A$  and  $A^*(nP)+B$  interactions, respectively. In addition, the measurable absorption signals in alkali-metal mixtures are smaller than in homoatomic alkali-metal vapors because the maximum number density  $N_{\text{max}}$  of the vapor is limited by the maximum buffer gas pressure (about 150 mbar in present

experiment) where the heat pipe can still operate in stable conditions. However, the present measurements showed that the reduced absorption coefficients for homo- and heteroatomic interactions were of the same order of magnitude. The relation  $k_R^{AA} \approx k_R^{AB}$  combined with the limited total vapor number density  $N_{\text{max}} = N_A + N_B$  yields the absorption coefficient  $k \approx k_R^{AA} N_{\text{max}} (N_{\text{max}} - N_B)$  which is obviously smaller than the corresponding absorption coefficient in homoatomic vapors. To minimize contributions by homoatomic reactions, it is desirable to have  $N_A \ll N_B$ . However, in such case, the heteroatomic term  $k_R^{AB} N_A N_B$  decreases too. Therefore, one needs to find a compromise for the  $N_A$  to  $N_B$  ratio which enables an optimum detection of the heteroatomic contributions. It turned out that the optimum conditions regarding the elimination of homoatomic contributions to the absorption were attained in mixtures with  $N_A/N_B \approx 1/3$ . However, at such optimum conditions the absorption signals due to heteroatomic interactions are significantly smaller (about 5 times) than the corresponding signals in pure vapors.

The individual number densities in the vapor mixtures were determined using absorption data of the corresponding diffuse bands of the dimers and the blue satellites of the second principal series lines as standards. With known number densities and known optical path  $L$ , the homoatomic contributions were calculated using the  $k_R^{AA}$  data presented in Figs. 4–6. Finally, the reduced absorption coefficients  $k_R^{AB}$  for the heteroatomic molecules were obtained by subtracting the calculated homoatomic contributions from the optical depths  $kL$  of the line wings.

The evaluation of the quasistatic wings of the potassium 4S- $nP$  series lines broadened by Rb or Cs was even more difficult. As one can see from the results presented below, the reduced absorption coefficients in the wings of self-broadened K 4S- $nP$  lines are generally smaller than in the case of the self-broadened Cs 6S- $nP$  and Rb 5S- $nP$  lines. The higher members of the potassium series are in the wavelength region below the limits of Cs and Rb principal series, i.e., the Cs 6S- $nP$  or Rb 5S- $nP$  lines do not blend higher K Rydberg series lines. However, the signal-to-noise ratio of the measured absorption in the quasistatic wings was insufficient to determine the contributions by heteroatomic interactions because of the limited detection sensitivity in vapor mixtures. It turned out that because of reduced sensitivity and line blending in alkali-metal mixtures, only a few lines of the  $A^*(nP)+B$  series could be measured with sufficient accuracy. These results are presented in Figs. 10 and 11.

The reduced absorption coefficients of the quasistatic wings of the third principal series line doublets of potassium and cesium broadened by rubidium are shown in Fig. 10. In comparison to the corresponding profiles caused by homoatomic reactions, the largest differences are in the red wings. There is the strong satellite due to K\*(6P)+Rb interaction placed between these two positions (at 347.8 nm) instead of the weak satellites at 346.9 and 348.3 nm in the case of self-broadened K 6P line. On the other hand, the far red satellite at 392 nm due to Cs\*(8P)+Cs interaction is stronger and shifted toward the doublet center in the Cs\*(8P)+Rb case.

The reduced absorption coefficients of the wings of the third and fourth Cs and Rb doublets broadened by K are

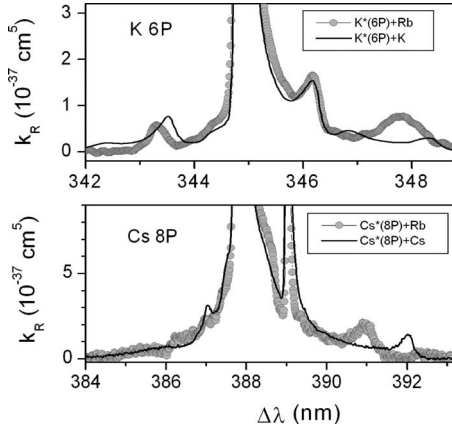


FIG. 10. The reduced absorption coefficients of the quasistatic wings of the K 4S-6P (top) and Cs 6S-8P (bottom) doublets broadened by Rb (gray dots). Heteroatomic broadening  $k_R^{ARb} = k/N_A N_{Rb}$  ( $A=K, Cs$ ) is compared to the corresponding homoatomic broadening ( $k_R^{AA} = k/N_A^2$ , black curves). The number densities in the K-Rb vapor mixture were  $N_K = 2.2 \times 10^{17} \text{ cm}^{-3}$  and  $N_{Rb} = 5.1 \times 10^{17} \text{ cm}^{-3}$ . In the Cs-Rb vapor mixture, the number densities were  $N_{Cs} = 2.7 \times 10^{17} \text{ cm}^{-3}$  and  $N_{Rb} = 4.8 \times 10^{17} \text{ cm}^{-3}$ .

given in Fig. 11. The far red satellites of the Cs 8P and 9P lines due to  $Cs^*(nP)+K$  interactions (Fig. 11 upper part) are shifted toward the line centers in comparison to the shapes of relevant self-broadened lines. As one can see from Fig. 10 (lower part) and Fig. 11 (upper part), the positions and the strengths of the far red satellites of the Cs 8P line broadened by Rb and K are nearly the same. The smallest differences between homo- and heteroatomic contributions to the profiles are observed for Rb 7P and Rb 8P lines broadened by potassium. The positions of the satellites and their strengths are almost identical within the experimental uncertainties.

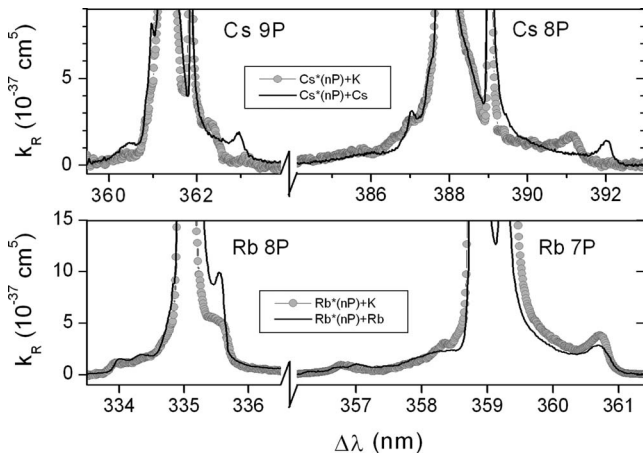


FIG. 11. The reduced absorption coefficients of the quasistatic wings of the Cs 6S-8P and 6S-9P (upper part) and Rb 5S-7P and 5S-8P (lower part) lines broadened by K (gray dots). The heteroatomic broadening  $k_R^{AK} = k/N_A N_K$  ( $A=Cs, Rb$ ) is compared to the corresponding homoatomic broadening ( $k_R^{AA} = k/N_A^2$ , black lines). The number densities in the Cs-K vapor mixture were  $N_{Cs} = 3.1 \times 10^{17} \text{ cm}^{-3}$  and  $N_K = 3.9 \times 10^{17} \text{ cm}^{-3}$ , while they were  $N_{Rb} = 1.5 \times 10^{17} \text{ cm}^{-3}$  and  $N_K = 4.5 \times 10^{17} \text{ cm}^{-3}$  in the Rb-K vapor mixture.

## VI. DISCUSSION

Comparing shapes, positions, and strengths of satellites, the K self-broadening data (Fig. 4) look very similar as the recently published Rb self-broadened principal series lines (Fig. 5) if one refers to lines with almost the same  $n_{eff}$ . This can also nicely be seen in Fig. 8 where sequences of three K and Rb lines with almost the same effective principal quantum numbers are compared. If the scattering of the valence electron is accepted to be the major mechanism for establishing the potential extrema, the value of the scattering length, representing the  $e^-$ -perturber interaction, is expected to be a measure for the relevant potential depths. Therefore, the similarities between the analyzed Rb and K spectra are not really surprising since the electron-scattering lengths on K and Rb are almost the same (K:  $\sim -11.5$  a.u., Rb:  $\sim -12.5$  a.u., see Refs. [11,13,22,23]). This is the reason why the adiabatic potentials of  $Rb_2$  and  $K_2$  Rydberg molecules should be virtually identical. This also means that the strong single blue satellites of the K  $nP$  lines ( $n_{eff} \approx 7.3, 8.3, 9.3$ , and higher) correspond to potential minima at interatomic distances  $R$ , i.e., at positions of the potential minima predicted by theory in [1–4]. These  $R$ 's are of the order of the radii of Rydberg atoms ( $\approx 1.5 \times n_{eff}^2$ ). On the other hand, the satellite structures measured in the wings of the self-broadened Cs principal series lines look different from the K and Rb cases at first glance (see Fig. 6). The satellites are spread over a larger energy range and there are more substructures than for K and Rb. Differences between Cs on one side and Rb and K on the other might be expected because the electron-scattering lengths of Cs (about  $-18$  a.u.) [11,13,22,23] is somewhat larger than of K and Rb. Furthermore, the fine structure of the Cs  $nP$  states is much larger than of comparable states in Rb and K and the oscillator strength ratio of the  $6S-nP_{3/2}$  and  $6S-nP_{1/2}$  deviates dramatically from 2 for Cs principal series Rydberg lines [24]. However, as the effective quantum number of the Cs lines is increasing, the structures of the lines become simpler and more comparable to the Rb and K lines. This can particularly be seen in the plot of the reduced absorption coefficients in dependence on  $n_{eff}$  in Fig. 8.

In general, with the decrease of the principal quantum number, the  $R$ -dependent oscillations of the calculated Born-Oppenheimer curves become stronger. This can be easily seen when the  $Rb_2^*$  potential curves for the principal quantum numbers of  $n \approx 30$  [1–3] and  $n \approx 10$  [6] are compared. This means that satellite structures should become richer and more pronounced for lower  $n$  values than for higher  $n$ . The outer red satellites correspond to the oscillations in the region of the global minima of the molecular potential curves belonging to the  $nP$  asymptotes. When  $n$  increases, the outer red satellites are closer to the line centers and form line shoulders when they are merging. The systematic behavior of the red wing shapes is especially evident in  $n_{eff}$  representations of the reduced absorption coefficients. Here, the distances  $\Delta n_{eff}$  between line centers and outer satellites (for lower  $n$ ) and accordingly line shoulders (for higher  $n$ ) are nearly constant and amount to about 0.17 and 0.19 for K and Rb, respectively. It has to be noted that the  $\Delta n_{eff}$  for Rb is in strong correlation with the spacing of the global potential

minima between the neighboring  $n$  manifolds calculated for trilobitelike systems [1–3]. Obviously, also the positions of the red outer satellites, representing the depths of the  $\text{Cs}_2$  Rydberg molecule potentials are also approaching an asymptotic value in the  $n_{\text{eff}}$  presentation for higher principal series lines as it is observed for  $\text{Rb}_2$  and  $\text{K}_2$  (see Fig. 8). It is interesting to note that the ratios of the  $\Delta n_{\text{eff}}$  values of Cs (0.29), Rb (0.19), and K (0.17) are very close to the respective ratios of the scattering lengths (see above).

The dominating influence of the electron-scattering lengths can also be seen in the broadening data of the heteroatomic systems. The line shapes and the satellite structures of the Rb  $7P$  and Rb  $8P$  lines broadened by K are almost identical to the shapes obtained in the Rb self-broadening experiment (lower part in Fig. 11). Even the potassium third principal series line, emerging from the low-lying K  $6P$  level, has one blue and one red satellites due to broadening by Rb at almost the same positions and with comparable strengths as the satellites observed in the K self-broadening experiment (see upper spectra in Fig. 10). On the other hand, the outer red satellites measured in the self-broadened Cs  $8P$  and  $9P$  lines are closer to the center of gravity of the lines than the red satellites measured in the neighborhood of the same lines with K as a perturber (see upper spectra of Fig. 11). The outer red satellites recorded in the self-broadened and Rb-broadened low-lying Cs  $8P$  lines (see lower spectra of Fig. 10) are different in position. The satellite in the heterocase is closer to the line center than the corresponding satellite in the Cs self-broadening experiment. Note that the positions of the outer red satellite in the wing of the Cs  $8P$  line broadened by Rb (lower spectrum in Fig. 10) and K (upper right spectrum in Fig. 11) are comparable in position, magnitude, and shape. This might also be taken as an indication that the electron-scattering lengths have influence on the relative positions of the outer red satellites, i.e., on the depths of the relevant molecular Rydberg potentials.

## VII. CONCLUSION

The presented line-shape measurements confirm that valence electron scattering in alkali-metal  $A^*+B$  systems is the dominant mechanism leading to the complicated satellite structures in the quasistatic wings for third and higher members of the principal series lines. Consequently, one can expect the existence of potential depths estimated by Eq. (2) and formation of bound  $A^*+B$  molecular states on the wide scale of principal quantum numbers starting from  $n_{\text{eff}}$  values larger than 4.

Taking into account the experimental results of the self-broadened Cs principal series lines, it would be highly desirable if theoretical calculations of  $\text{Cs}_2$  trilobite and butterfly states are performed since they show the most pronounced and deepest potential minima of all alkali-metal Rydberg molecules. Therefore,  $\text{Cs}_2$  Rydberg molecules would be ideal candidates for stepwise laser excitation of vibrational states in ultracold molecules which have smaller vibrational energy spacings than in the case of  $\text{Rb}_2$  Rydberg molecules. Furthermore, it would also be very interesting to study intermediate states of ultracold alkali-metal Rydberg molecules, e.g., around effective principal quantum numbers of about 12–20 where the natural lifetimes are well above  $1 \mu\text{s}$  [25–28]. Here, the potential depths are much deeper than for high-lying states and the multiple potential minima could also be studied in detail.

## ACKNOWLEDGMENTS

The presented investigations were obtained within the frame of Project No. 035-0352851-2853 financially supported by the Ministry of Science, Education, and Sports of the Republic of Croatia. Financial supports by the Deutsche Forschungsgemeinschaft (Project no. 436 KRO 113/9/0-1), the Ministry of Innovation, Science, Research, and Technology of the state North Rhine Westphalia, and the Ministry of Education and Research of the Federal Republic of Germany are gratefully acknowledged.

- 
- [1] C. H. Greene, A. S. Dickinson, and H. R. Sadeghpour, Phys. Rev. Lett. **85**, 2458 (2000).
  - [2] B. E. Granger, E. L. Hamilton, and C. H. Greene, Phys. Rev. A **64**, 042508 (2001).
  - [3] E. L. Hamilton, C. H. Greene, and H. R. Sadeghpour, J. Phys. B **35**, L199 (2002).
  - [4] A. A. Khuskivadze, M. I. Chibisov, and I. I. Fabrikant, Phys. Rev. A **66**, 042709 (2002).
  - [5] I. C. H. Liu, J. Stanojevic, and J. M. Rost, Phys. Rev. Lett. **102**, 173001 (2009).
  - [6] C. H. Greene, E. L. Hamilton, H. Crowell, C. Vadla, and K. Niemax, Phys. Rev. Lett. **97**, 233002 (2006).
  - [7] N. Allard and J. Kielkopf, Rev. Mod. Phys. **54**, 1103 (1982).
  - [8] J. Szudy and W. E. Baylis, Phys. Rep. **266**, 127 (1996).
  - [9] V. V. Eliseev and G. V. Sholin, Opt. Spectrosc. **30**, 222 (1971).
  - [10] K. Niemax, Phys. Lett. **38A**, 141 (1972).
  - [11] H. Heinke, J. Lawrenz, K. Niemax, and K. H. Weber, Z. Phys. A **312**, 329 (1983).
  - [12] B. P. Stoicheff and E. Weinberger, Phys. Rev. Lett. **44**, 733 (1980).
  - [13] I. I. Fabrikant, J. Phys. B **19**, 1527 (1986).
  - [14] V. Bendkowsky, B. Butscher, J. Nipper, J. P. Shaffer, R. Löw, and T. Pfau, Nature (London) **458**, 1005 (2009).
  - [15] C. Vadla, R. Beuc, V. Horvatic, M. Movre, A. Quentmeier, and K. Niemax, Eur. Phys. J. D **37**, 37 (2006).
  - [16] V. Horvatic, R. Beuc, M. Movre, and C. Vadla, J. Phys. B **26**, 3679 (1993).
  - [17] T. Ban, H. Skenderovic, R. Beuc, I. Krajcar Bronic, S. Rousseau, A. R. Allouche, M. Aubert-Frécon, and G. Pichler, Chem. Phys. Lett. **345**, 423 (2001).
  - [18] T. Ban, R. Beuc, H. Skenderovic, and G. Pichler, Europhys. Lett. **66**, 485 (2004).

- [19] S. Magnier, M. Aubert-Frécon, and A. R. Allouche, *J. Chem. Phys.* **121**, 1771 (2004).
- [20] C. Vadla, V. Horvatic, and K. Niemax, *Appl. Phys. B: Lasers Opt.* **84**, 523 (2006).
- [21] W. Hansen, *J. Phys B* **17**, 4833 (1984).
- [22] C. Bahrim, U. Thumm, and I. I. Fabrikant, *J. Phys. B* **34**, L195 (2001).
- [23] D. C. Thompson, E. Weinberger, G.-X. Xu, and B. P. Stoicheff, *Phys. Rev. A* **35**, 690 (1987).
- [24] C.-J. Lorenzen and K. Niemax, *J. Phys. B* **11**, L723 (1978).
- [25] Z. G. Feng, L. J. Zhang, J. M. Zhao, C. Y. Li, and S. T. Jia, *J. Phys. B* **42**, 145303 (2009).
- [26] T. F. Gallagher and W. E. Cooke, *Phys. Rev. A* **20**, 670 (1979).
- [27] M. Hugon, F. Gounand, and P. R. Fournier, *J. Phys. B* **11**, L605 (1978).
- [28] J. Marek and K. Niemax, *J. Phys. B* **9**, L483 (1976).